Int. J. Electrochem. Sci., 15 **(2020)** 8849 – 8872, doi: 10.20964/2020.09.64

International Journal of
ELECTROCHEMICAL
SCIENCE
www.electrochemsci.org

Thermodynamic Performance Evaluation on a Molten Hydroxide Direct Carbon Fuel Cell with Asymmetric Anode and Cathode

Yuan Han[1], *Houcheng Zhang*[1,*], *Ziyang Hu* [1], *Shujin Hou*[2,*]

[1] Department of Microelectronic Science and Engineering, Ningbo University, Ningbo 315211, China
[2] College of Physics and Electronic Engineering, Nanyang Normal University, Nanyang 473061, China
[*]E-mail: zhanghoucheng@nbu.edu.cn (H. Zhang); houshujingrb@163.com (S. Hou).

Received: 2 May 2020 / *Accepted:* 13 July 2020 / *Published:* 10 August 2020

The asymmetric electrode configuration can effectively solve the electrolyte carbonation problem for molten hydroxide direct carbon fuel cells (MHDCFCs), however, the thermodynamic performance of this kind of MHDCFC has not been well understood yet. Herein, an MHDCFC model with active carbon as fuel and molten sodium hydroxide (NaOH) as electrolyte is proposed, in which the anode and cathode are asymmetric. According to the electrochemical reaction kinetics, electrode process and mass transfer, various irreversible losses of the electrochemical process are described. Considering diverse polarization losses, the thermodynamic performance of the MHDCFC is comprehensively evaluated by using output voltage, efficiency, power output, entropy production rate, ecological objective function and ecological coefficient of performance as objective functions. The MHDCFC model is validated to be reliable by comparing with previous modeling results. The generic performance characteristics of the MHDCFC are revealed. The effects of the operating temperature, anodic and cathodic chamber heights, fuel mass, O_2 flow rate, cathodic pressure, and reaction chamber width on the MHDCFC performance are analyzed through exhaustive parametric studies. The obtained results may provide some insights into globally understanding the performance of MHDCFCs.

Keywords: Molten hydroxide direct carbon fuel cell; Efficiency; Power output; Ecology objective function; Ecological coefficient of performance

1. INTRODUCTION

Hydrogen fuel cells have been paid more and more attention because they are clean and efficient. However, considering the degree of social acceptance and the cost and technology of producing hydrogen [1-2], the arrival of the hydrogen energy era still needs some time [2, 3]. At the present stage, coal resources are still in a dominant position because they are abundant and inexpensive [3]. Compared

with hydrogen, solid carbon fuels can be easily obtained by simply processing of coal. In addition, solid carbon fuels are convenient for transportation or storage due to their small volume and high calorific value [4]. Thus, it is urgent to explore an efficient and clean way for coal utilization because of the fossil fuel shortage and environmental pollution. In this context, direct carbon fuel cells (DCFCs) have attracted widespread attention all over the world. DCFCs enable to directly transform the chemical energy stored in solid carbon into electricity without any fuel reforming or combustion process, and the produced carbon dioxide can be conveniently captured and stored. Furthermore, DCFCs offer higher theoretical efficiency than traditional hydrogen fuel cells [5-8].

Depending on the electrolyte types, DCFCs can be mainly divided into molten carbonate direct carbon fuel cells (MCDCFCs) [9-11], molten hydroxide direct carbon fuel cells (MHDCFCs) [12-14], and solid oxide direct carbon fuel cells (SODCFCs) [14-17]. Among these DCFCs, MHDCFCs have drawn more and more interest because of lower working temperature, higher current density and higher fuel utilization and etc. Furthermore, the kinetics of Boudouard reaction ($CO_2+C=2CO$) is strongly limited under low-temperature conditions [3, 18, 19]. Therefore, a higher purity of CO_2 product and higher power generation efficiency can be expected [20, 21]. However, the molten hydroxide electrolyte is easily carbonized, which may significantly degrade the performance of MHDCFC [22]. The electrolyte may be carbonated in two ways: $C + 6OH^- = CO_3^{2-} + 3H_2O + 4e^-$ or $2OH^- + CO_2 = CO_3^{2-} + H_2O$ [23-30]. It is widely accepted that electrolyte carbonation is caused by $2OH^- + CO_2 = CO_3^{2-} + H_2O$, in which carbon dioxide produced from the anode is not discharged in time while reacts with the electrolyte [31-34]. Hence, a lower anode chamber height can relieve the electrolyte carbonation by curtailing the residence time of carbon dioxide [35-38].

To commercialize MHDCFCs, considerable studies have been carried out on various aspects, including the corrosion [14], fuel treatment [28], carbonate formation [30] and performance optimization [39]. For example, Guo et al. [14] developed an MHDCFC with the aim to minimize corrosion of both fuel cell materials and fuel carbon. Kacprzak et al. [28] experimentally tested various carbonaceous fuels for MHDCFC and found that the raw coal displayed the best performance among the four tested fuels. Zecevic et al. [30] successively built four MHDCFC prototypes to overcome the carbonate formation issues. Xing et al. [39] electrochemically modeled an MHDCFC by taking the activation polarization loss, concentration polarization loss and ohmic polarization loss as the main voltage reduction sources. However, the effects of some designing parameters such as reaction chamber width on the cell performance are still unknown, especially the thermodynamic performance.

Thermodynamics theory has been a useful tool for optimizing the performance of various thermodynamic cycles, thermal systems, and emerging energy converters [40-42]. The thermodynamic performance can be evaluated by various objective functions, including the energy efficiency, exergy efficiency, power output and entropy generation rate [40-44]. In addition, ecological objective function (EOF) and ecological coefficient of performance (ECOP) are also widely used as objective functions because they can evaluate the thermodynamic performance considering both power output and loss rate of availability [43-48]. Obviously, it is meaningful to assess the MHDCFC performance under various conditions using multiple optimization criteria, which will help to globally understand the

thermodynamic performance. However, there is no study reported on this topic in the current literatures yet.

In this paper, comprehensive thermodynamic performance evaluation on an irreversible MHDCFC with asymmetric electrodes will be conducted. The MHDCFC model will be detailedly described by including the electrochemical losses such as activation polarization loss, concentration polarization loss and ohmic polarization loss. Based on the theory of thermodynamics, some important performance parameters such as output voltage, efficiency, power output, entropy production rate, EOF and ECOP will be formulated to evaluate the performance of MHDCFC. The impacts of some decisive designing parameters and operating conditions on the comprehensive MHDCFC performance will be discussed through exhaustive parametric studies.

2. MODEL DESCRIPTION

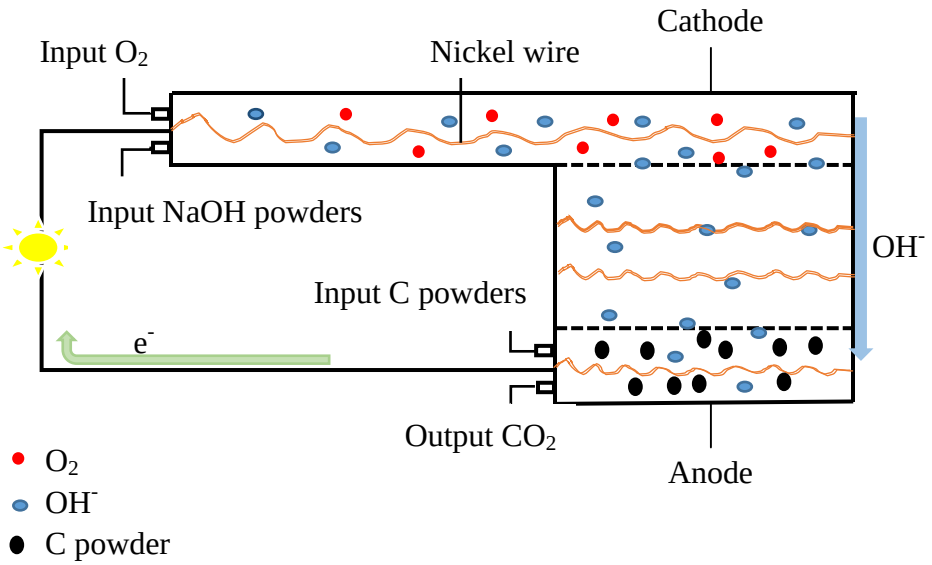

Figure 1. Schematic diagram of an MHDCFC.

Figure 1 schematically shows that the MHDCFC comprises an anodic chamber, a molten NaOH electrolyte and a cathodic chamber, where the height of the anodic chamber is significantly lower than that of the cathodic chamber. A higher cathodic chamber lengthens the oxygen reaction path, which guarantees that the oxygen is sufficient. Nickel wires doped with lithium inside the anodic and cathodic chambers function as electrode, current collector and catalyst, and wherein, a small amount of lithium doped in nickel can effectively prevent nickel from being oxidized [49, 50]. The solid carbon fuel indirectly contacts with the nickel anode. A porous plate with many small holes seals the two electrode chambers and prevents both oxygen and fuel from leaking into the electrolyte chamber. Carbon particles are introduced into the anodic chamber and the NaOH powders are introduced into the cathodic chamber. After a heating process, the temperature exceeds the melting point of NaOH, and the NaOH electrolyte

melts and moves from cathodic chamber to anodic chamber through the porous plate, eventually filling the whole reactor. The humidified oxygen is fed into the cathodic chamber with an optimum and constant rate. The consumption rates of carbon and oxygen can be calculated by detecting the amount of CO_2 produced at the anodic chamber. Therefore, carbon fuel and oxygen can be accurately and continuously fed to ensure the continuous and stable power output of MHDCFC.

The wetted O_2 molecules diffuse into the cathodic chamber where they are reduced into hydroxide ions (OH^-) with the assistance of the electrons [51], i.e.,

$$O_2 + 2H_2O + 4e^- = 4OH^- \quad (1)$$

The generated OH^- is transported through the molten NaOH electrolyte to the anodic chamber and reacts with carbon fuel to produce H_2O and CO_2. The carbon fuel in the anodic chamber loses four electrons, and the electrochemical reaction can be expressed as [52]

$$C + 4OH^- = 2H_2O + CO_2 + 4e^- \quad (2)$$

The total chemical reaction in MHDCFC is that the chemical energies stored in carbon and oxygen are converted into electrical and thermal energies, i.e.,

$$C + O_2 = CO_2 + \text{electricity} + \text{heat} \quad (3)$$

To simplify the subsequent analyses, the following assumptions are adopted [8, 20, 22, 34, 35, 39]:

(1) The MHDCFC operates stably, and the carbon fuel is evenly distributed in the reaction chamber;

(2) The number of holes in the porous plate of the sealed compartment is enough, and the electrolyte can penetrate the cathodic and anodic chambers;

(3) Only complete oxidation of carbon occurs in the MHDCFC, and the two-electron process of CO formation by partial oxidation of carbon is neglected;

(4) The carbon dioxide produced at the anodic chamber is discharged in time without any electrolyte carbonation;

(5) The interconnection conductivity between carbon fuel and NaOH electrolyte is neglected;

(6) Both operating temperature and fuel have no effect on the electrical conductivity of NaOH electrolyte.

In the MHDCFC, the total energy released by the electrochemical reaction can be expressed by [13]

$$-\Delta H = -\Delta G - T\Delta S \quad (4)$$

where ΔH is the enthalpy change, ΔG is the Gibbs free energy change; ΔS is the entropy change; T is the operating temperature. Theoretically, the thermal efficiency $\Delta G/\Delta H$ of MHDCFC is almost 100% in the range of typical operating temperature [3].

Based on the Faraday's law, the rate of total energy released is [53]

$$-\Delta \dot{H} = -\frac{\Delta h I}{n_e F} \quad (5)$$

where n_e is the number of electrons per carbon molecular involving the reaction ($n_e = 4$); F is the Faraday constant; I is the operating electric current of MHDCFC [54, 55]; and Δh is the molar enthalpy change.

According to the Nernst equation, the open circuit voltage (OCV) at a given temperature and gas concentrations is given by [55-59]

$$V = V_0 + \frac{RT}{n_e F}\ln(\frac{P_{O_2,cat}}{P_{CO_2,an}}) \quad (6)$$

where R, $P_{O_2,cat}$ and $P_{CO_2,an}$ are, respectively, the general gas constant, partial pressure of O_2 at the cathodic chamber and partial pressure of CO_2 at the anodic chamber; V_0 is the ideal potential under the standard conditions, which is given by [55]

$$V_0 = \frac{-\Delta g^0}{n_e F} \quad (7)$$

where Δg^0 is the standard molar Gibbs free energy change of the electrochemical reaction (3).

When the MHDCFC works, the actual output voltage V_{cell} is always lower than V due to the electrode dynamics, reactants (or products) transportation and electrical (or ionic) resistance of MHDCFC assembly. These irreversible losses can be characterized by activation polarization loss (E_{act}), concentration polarization loss (E_{con}) and ohmic polarization loss (E_{ohm}). In the following, each polarization loss will be described.

(1) Activation polarization loss

The relationship between the activation polarization loss and the operating current density can be calculated by the general Butler-Volmer equation [59], i.e.,

$$J = J_{0,m}\left[\exp\left(\frac{\delta n_e F E_{act,m}}{RT}\right) - \exp\left(\frac{-(1-\delta) n_e F E_{act,m}}{RT}\right)\right] \qquad (m = \text{an or cat}) \quad (8)$$

where J is the operating current density; $J_{0,m}$ is the exchange current density of anode or cathode; $E_{act,m}$ is the activation polarization loss of anode or cathode; δ is the electrochemical transfer coefficient (δ=0.5) [22, 54].

The anodic or cathodic activation polarization loss can be further expressed as [8, 20, 33]

$$E_{act,m} = \frac{RT}{2F}\ln\left[\frac{J}{2J_{0,m}} + \sqrt{\left(\frac{J}{2J_{0,m}}\right)^2 + 1}\right] \quad (9)$$

where the anode exchange current density and cathode exchange current density can be, respectively, expressed as [7]

$$J_{0,an} = 1.252\times10^{11}\exp\left(\frac{-22175}{T}\right) \quad (10)$$

and

$$J_{0,\text{cat}} = 7.8\times\exp\left[\frac{5800(T-923)}{923T}\right]\left(P_{O_2,,cat}\right)^r \quad (11)$$

where r represents the exponent of O_2 partial pressure, and its value is set as 0.625 [54].

(2) Concentration polarization loss

Concentration polarization loss is caused by the transportation resistance when a substance approaches or leaves the reaction sites [39]. Since the carbon fuels are always abundant in the anodic

chamber, the anodic concentration polarization can be safely ignored. The concentration polarization loss mainly refers to cathodic concentration polarization losses and can be expressed as [55- 62]

$$E_{con} = \frac{RT}{n_e F} \ln\left(\frac{J_{\lim}}{J_{\lim} - J}\right) \quad (12)$$

where $J_{\lim}$ is the limiting current density, which can be further expressed as

$$J_{\lim} = n_e FKC \quad (13)$$

where K is the mass transfer coefficient; C is the oxygen concentration in the cathodic chamber; and they can be, respectively, expressed as [42]

$$K = 1.875 v Re^{0.55} Sc^{2/3} \quad (14)$$

and

$$C = P_{O_2,cat}\left\{\frac{1}{k(C_1)^y + 1}\right\}^b f(T) \quad (15)$$

where v is the O_2 flow rate, Sc is the Schmidt number; C_1 is the NaOH concentration in pure water and its value is 24.75 [42]; y and b are two exponents; k is a coefficient; and Re and $f(T)$ are the Reynolds number [63] and temperature-dependent function [43], which can be, respectively, expressed as

$$Re = \frac{vd}{V_1} \quad (16)$$

$$f(T) = \exp\left\{\frac{0.046T^2 + 203.35T\ln(T/298) - (299.378 + 0.092T)(T - 298) - 20.591\times10^3}{8.3144T}\right\} \quad (17)$$

where d is the cathodic chamber effective diameter, and V_1 is the kinematic viscosity.

(3) Ohmic polarization loss

Ohmic polarization loss is resulted from the resistances of electrolyte, electrode as well as connection wires, which follows the Ohm's law. The anodic chamber resistance R_{an} can be expressed as [39]

$$R_{an} = \frac{X_{an}}{\alpha_{an} Y H_1} \quad (18)$$

where Y, X_{an} and H_1 are, respectively, the width, length and height of the anodic chamber; and α_{an} is the apparent anode conductivity, which can be written as [40]

$$\alpha_{an} = \alpha_{an}^{\ 0}(1 - \varepsilon_{an})^{1.5} \quad (19)$$

where α_{an}^0 and ε_{an} are pure anode fuel conductivity and anode particle holdup, respectively. ε_{an} can be further calculated by

$$\varepsilon_{an} = \frac{M_{an}}{\rho_{an} A H_1} \quad (20)$$

where ρ_{an}, A and M_{an} are, respectively, the actual density of anode, bed cross-sectional area and fuel mass.

Similarly, the cathodic chamber resistance R_{cat} can be given by [62]

$$R_{cat} = \frac{X_{cat}}{\alpha_{cat} Y H_2} \tag{21}$$

where

$$\alpha_{cat} = {\alpha_{cat}}^0 \left(1 - \varepsilon_{cat}\right)^{1.5} \tag{22}$$

$$\varepsilon_{cat} = \left\{2 + \left(0.35/v\right)\left[\left(\rho/1000\right)\left(\lambda/0.072\right)\right]^{1/3}\right\}^{-1} \tag{23}$$

$$\lambda = \begin{cases} 0.02645T + 115.2 & \left(623\,\mathrm{K} < T \le 723\,\mathrm{K}\right) \\ -0.01214T + 143.1 & \left(723\,\mathrm{K} < T < 823\ \mathrm{K}\right) \\ -0.203T + 293 & \left(823\,\mathrm{K} \le T < 973\ \mathrm{K}\right) \end{cases} \tag{24}$$

X_{cat}, Y and H_2 are, respectively, the length, width and height of the cathodic chamber; α_{cat} is the apparent cathode conductivity; α_{cat}^0 is the pure cathode conductivity; ε_{cat} is the cathode gas holdup; ρ and λ are the density of molten NaOH and surface tension of the electrolyte, respectively. The typical parameters can be found in Table 1.

Therefore, the total resistance and ohmic polarization loss of MHDCFC can be, respectively, given by

$$R_{ohm} = R_{an} + R_{cat} \tag{25}$$

and

$$E_{ohm} = JR_{ohm} \tag{26}$$

Thus, the output voltage V_{cell} can be expressed as

$$V_{cell} = V - E_{act,an} - E_{act,cat} - E_{con} - E_{ohm} \tag{27}$$

The power output, efficiency and entropy production rate of the MHDCFC can be, respectively, expressed as [42]

$$P = V_{cell} I \tag{28}$$

$$\eta = \frac{P}{-\dot{\Delta H}} = \frac{-n_e F V_{cell}}{\Delta h} \tag{29}$$

and

$$\sigma = \left(-\dot{\Delta H} - P\right)\frac{1}{T_0} = \left(-\frac{\Delta h}{n_e F} - V_{cell}\right)\frac{I}{T_0} \tag{30}$$

where T_0 is the environment temperature.

Furthermore, the EOF and ECOP of MHDCFC can be, respectively, expressed as [44-47]

$$E = P - T_0\sigma = V_{cell} I - T_0\sigma \tag{31}$$

and

$$ECOP = \frac{P}{T_0\sigma} = \frac{V_{cell} I}{T_0\sigma} \tag{32}$$

Table 1. Parameters used in the modeling.

Parameters	Values
Partial pressure of O_2 in cathodic chamber ($P_{O_2,cat}$)	2.0 atm
Partial pressure of CO_2 in anodic chamber ($P_{CO_2,an}$)	2.1 atm
Length of reaction chamber (X_{an}, X_{cat})	0.02 m
Width of anodic or cathodic chamber (Y)	0.15 m
Height of anodic chamber (H_1)	0.06 m
Height of cathodic chamber (H_2)	0.2 m
Effective diameter of cathodic chamber (d)	0.06 m
Electrolyte	NaOH
Operation temperature (T)	900 K
Environment temperature (T_0)	298 K
Density of activated carbon (ρ_{an})	2134 kg m^{-3} [39]
Density of electrolyte (ρ)	2130 kg m^{-3}
Exponent of O_2 pressure (r)	0.625 [55]
Charge transfer coefficient (δ)	0.5 [7]
Conductivity of activated carbon (α_{an}^0)	29300 S m^{-2} [7]
Conductivity of cathode (α_{cat}^0)	3800 S m^{-2} [7]
Schmidt number (Sc)	1000 [55]
Kinematic viscosity (V_1)	2.23×10^{-6} m^2 s^{-1} [63]
Mass of the MHDCFC in the anodic chamber M_{an}	0.01 kg
O_2 flow rate (v)	0.11 m s^{-1}
k	0.102078 [39]
m	4.308933 [39]
y	1.00044 [39]

3. RESULTS AND DISCUSSION

In this section, whether the present model is good or not will be checked. In addition, how the thermodynamic performance of MHDCFC is affected by various designing parameters and operating conditions will be also discussed by comprehensive parametric studies.

3.1. Model validation

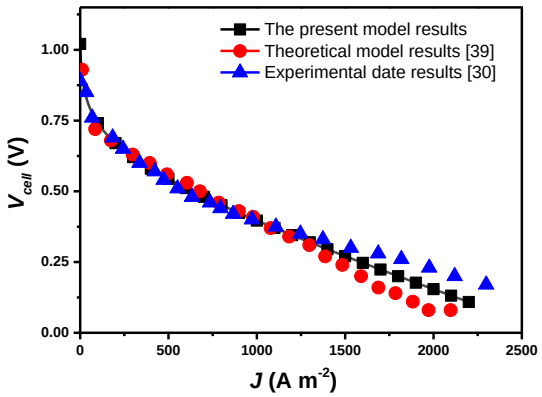

Figure 2. Comparisons between the present MHDCFC modeling results and the theoretical model results obtained by Xing's et al. [39] and experimental results obtained by Kacprzak's et al. [30].

To validate the present MHDCFC model, the output voltage of the present MHDCFC model is compared with that of Xing's model [39] and Kacprzak's experimental date [30], as shown in Fig. 2. It is seen that the output voltages decrease with an increase in the operating current density. Additionally, Fig. 2 clearly displays that a good consistency between the present modeling results and the theoretical modeling results and the experimental results, except in the higher operating current density region. This is because the fuel cell output voltage in the higher operating current density region is mainly governed by the concentration overpotential, which is related to various design parameters and operating conditions. Meanwhile, the discrepancy between the present MHDCFC model and the Xing's model [39] and Kacprzak's date [30] is very small, indicating that the present MHDCFC model is reliable and valid to predict the performance of an actual MHDCFC.

3.2. Effect of operating temperature

As illustrated in Fig. 3, the output voltage, efficiency, output power density, specific EOF and ECOP increase as the operating temperature rises, while the specific entropy production rate decreases as the operating temperature increases. The range of operating current density is enlarged as the MHDCFC operating temperature is higher. This is because the electrodes of MHDCFC are more reactive and the mass transfer within the MHDCFC is improved at higher operating temperatures, leading to a lower polarization loss and a larger output voltage. As shown by Eqs. (28)-(32), a larger output voltage

results in an increase in efficiency, output power density, specific EOF and ECOP and a decrease in specific entropy production rate. Fig. 3 also illustrates that both efficiency and ECOP are monotonically decreasing functions of the operating current density, while the output power density and specific EOF first increase and then decrease with an increase in the operating current density. Therefore, there exist a maximum power output density P^*_{max} and a maximum specific EOF E^*_{max}, and the corresponding current densities at P^*_{max} and E^*_{max} are J_P and J_E, respectively. It is observed that P^*_{max}, E^*_{max}, J_P and J_E shift to larger ones as the operating temperature grows.

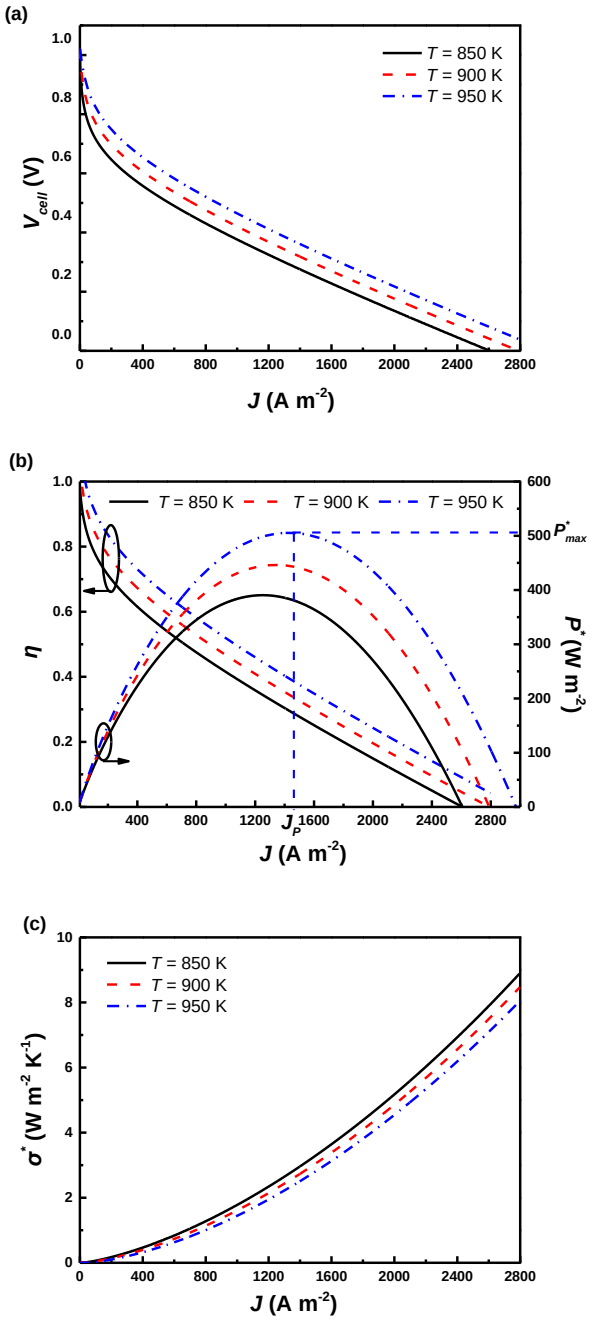

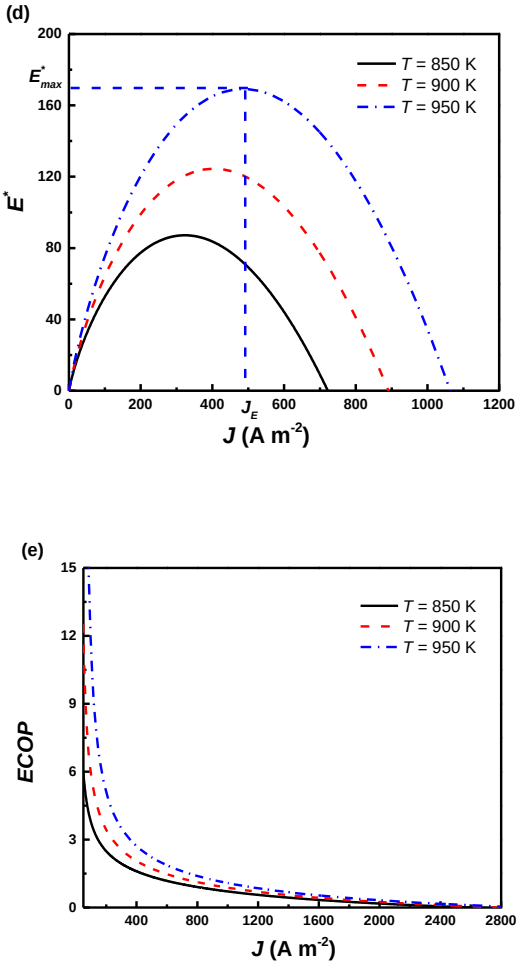

Figure 3. Effects of operating temperature on (a) output voltage, (b) efficiency and output power density, (c) specific entropy production rate, (d) specific EOF, and (e) ECOP, where $P^* = P/A$ is the output power density, and J_P is the current density corresponding to the maximum output power density P^*_{max}; $\sigma^* = \sigma/A$ is the specific entropy production rate; $E^* = E/A$ is the specific EOF, and J_E is the operating current density corresponding to the maximum specific EOF E^*_{max}.

Furthermore, both efficiency and power output density decrease as the operating current density increases in the region $J > J_P$. Obviously, the region of $J > J_P$ is not an optimum one for the MHDCFC system. Therefore, the optimum operating current density region is situated in the region of $0 < J < J_P$. In general, a higher working temperature is more conducive to MHDCFC performance.

3.3. Effect of anodic and cathodic chamber heights

As depicted in Fig. 4, the output voltage, efficiency, output power density, specific EOF and ECOP of MHDCFC increase with the increase of the anodic height or cathodic height, while the ohmic polarization loss and specific entropy production rate decrease as the anodic height or cathodic height increases. This is because the anode particle holdup decreases while the apparent anode conductivity

increases as anodic height increases, which leads to a smaller anodic chamber resistance. Furthermore, the anodic ohmic polarization loss is in inversely proportional to the anodic chamber resistance while the output voltage is in proportional to the anodic chamber resistance. As shown by Eq. (21), the cathodic chamber resistance decreases with the increase of the cathodic height, which results in a smaller cathodic ohmic polarization loss and a larger output voltage.

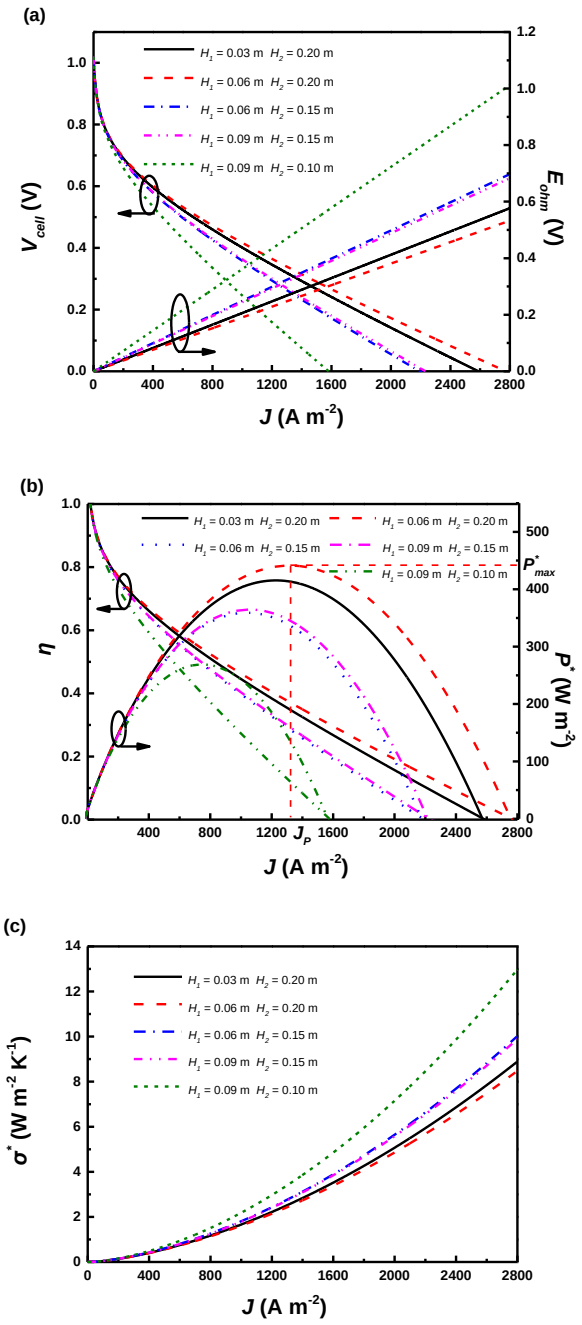

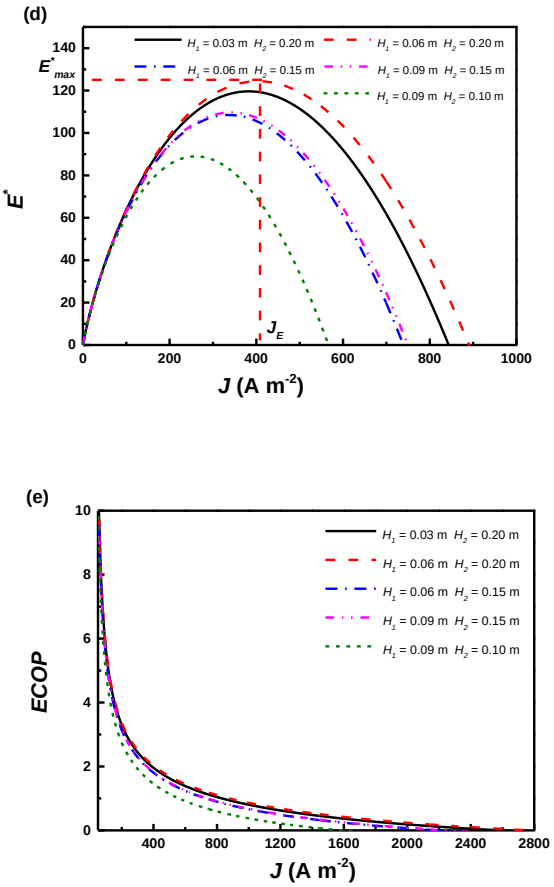

Figure 4. Effects of anodic and cathodic chamber heights on (a) output voltage and ohmic polarization loss, (b) efficiency and output power density, (c) specific entropy production rate, (d) specific EOF, and (e) ECOP, where the operating temperature T = 900 K.

Fig. 4 also shows that the effects of anodic and/or cathodic heights on the MHDCFC performance get more prominent with the increasing operating current density. Additionally, the operating current density range of the MHDCFC as well as J_P and J_E increase with an increase in the anodic height or cathodic height.

3.4. Effect of fuel mass

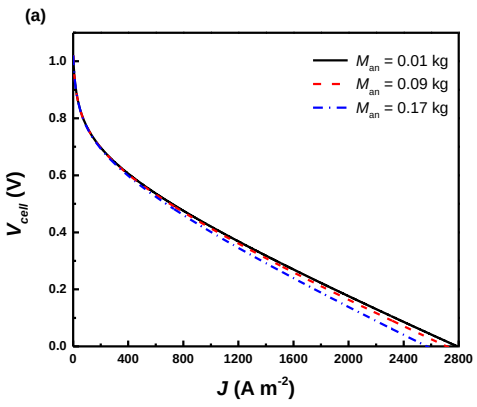

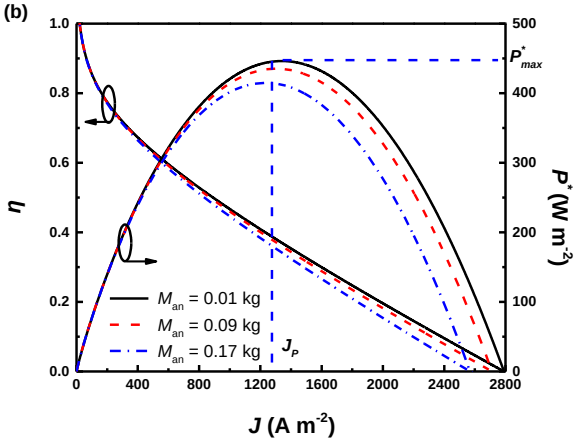
(b)
η
P* (W m-2)
P*max
JP
Man = 0.01 kg
Man = 0.09 kg
Man = 0.17 kg
J (A m-2)

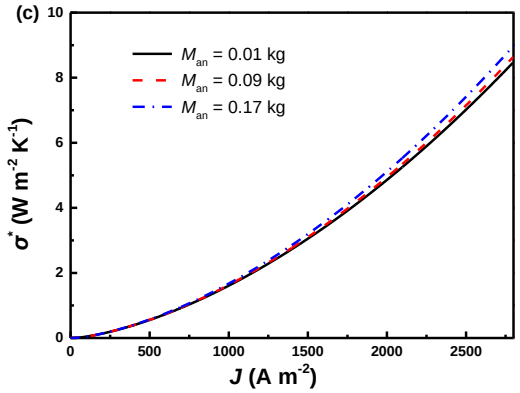
(c)
σ* (W m-2 K-1)
Man = 0.01 kg
Man = 0.09 kg
Man = 0.17 kg
J (A m-2)

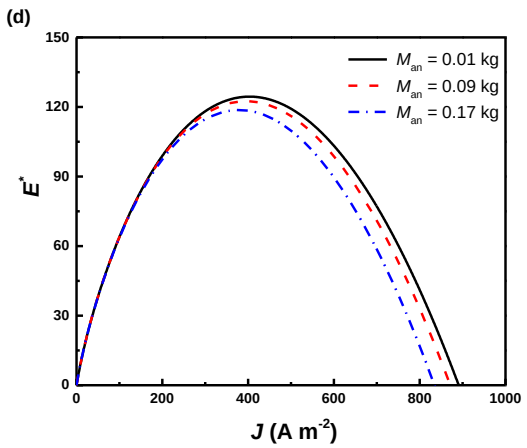
(d)
E*
Man = 0.01 kg
Man = 0.09 kg
Man = 0.17 kg
J (A m-2)

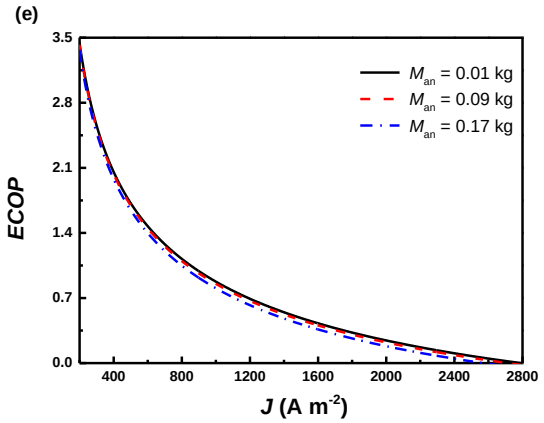

Figure 5. Effects of fuel mass on (a) output voltage, (b) efficiency and output power density, (c) specific entropy production rate, (d) specific EOF, and (e) ECOP, where H_1 = 0.06 m, H_2 = 0.2 m.

Fig. 5 depicts that the output voltage, efficiency, output power density, specific EOF and ECOP of MHDCFC decrease with the increase of the fuel mass, while the specific entropy production rate increases as the fuel mass increases. As shown by Eqs. (18) – (20), the anode particle holdup and anodic chamber resistance are increased with the increasing fuel mass, which lead to a larger ohmic polarization loss and a smaller output voltage. Furthermore, the smaller output voltage results in a decrease in efficiency, output power density, specific EOF and ECOP. In addition, J_P and J_E decrease as the fuel mass increases. The effects of fuel mass on the MHDCFC performance become more sensitive as the operating current density increases. Although a smaller fuel mass benefits the MHDCFC performance, it is unsatisfactory to continuously and large-scalely produce electricity.

3.5. Effect of O_2 flow rate

Fig. 6 illustrates that the output voltage, concentration polarization loss, efficiency, output power density, specific EOF and ECOP of MHDCFC decrease with an increase in the O_2 flow rate, while the ohmic polarization loss and specific entropy production rate increase as the O_2 flow rate grows. This is because a larger O_2 flow rate increases both the limiting current density and the mass transfer coefficient, which lead to an increase in the output voltage and a decrease in the concentration polarization loss. In addition, a larger O_2 flow rate not only decreases the oxygen concentration difference in the cathodic chamber but also increases the apparent cathode conductivity and the collision between oxygen molecules and cathodic chamber wall, which lead to an increase in the cathodic ohmic polarization loss and a decrease in the output voltage.

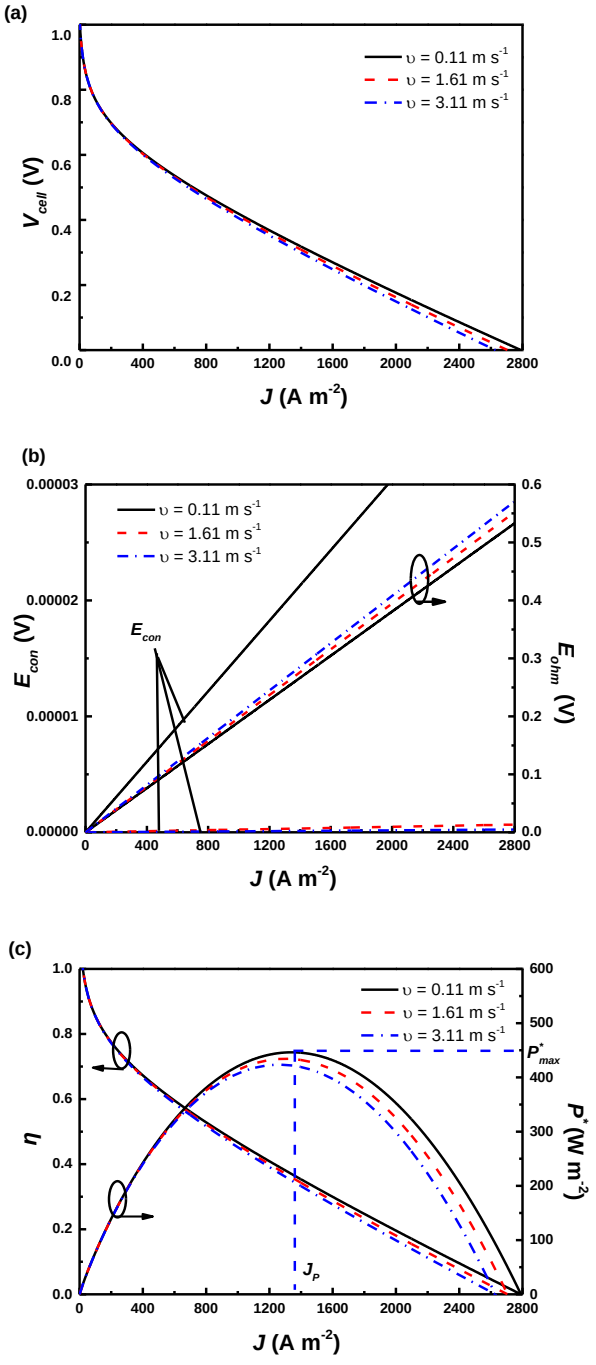
(a)
υ = 0.11 m s-1
υ = 1.61 m s-1
υ = 3.11 m s-1
Vcell (V)
J (A m-2)
(b)
Econ
Econ (V)
Eohm (V)
(c)
η
P*max
P* (W m-2)
JP

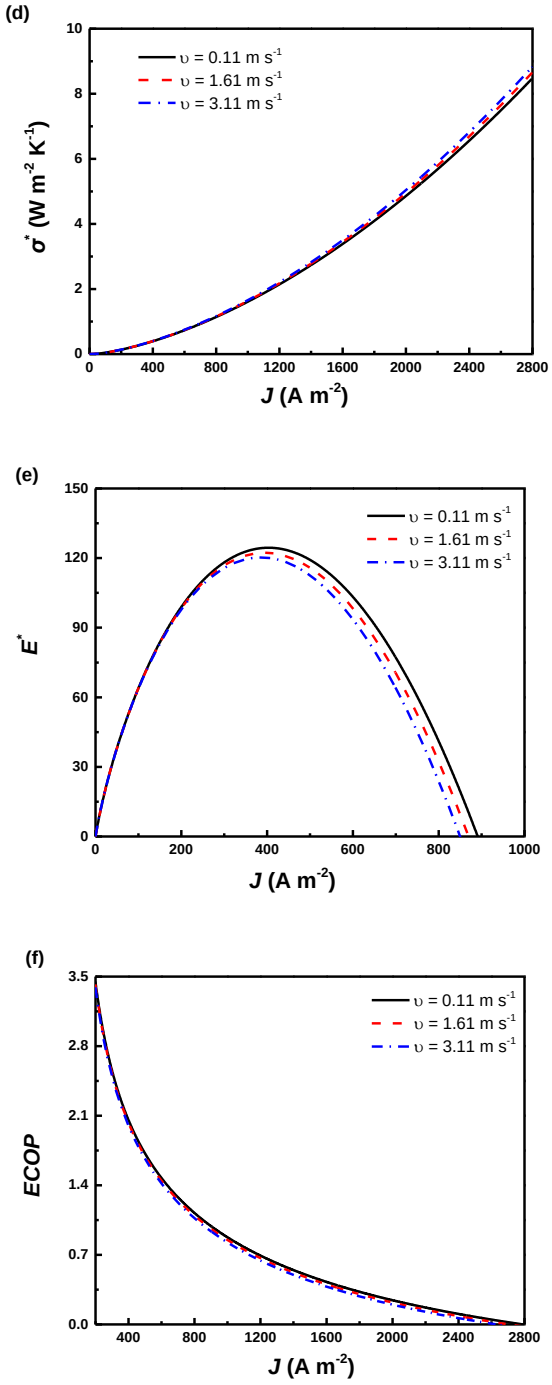

Figure 6. Effects of O_2 flow rate on (a) output voltage, (b) concentration polarization loss and ohmic polarization loss, (c) efficiency and output power density, (d) specific entropy production rate, (e) specific EOF, and (f) ECOP.

Since the impacts of O_2 flow rate on concentration polarization loss is smaller than that on ohmic polarization loss, a higher O_2 flow rate will degrade the MHDCFC performance. Furthermore, the effects of O_2 flow rate on the MHDCFC performance become insensitive at small operating current densities. This is because the rate of oxygen consumption is smaller than that of oxygen supply at small operating current densities, and therefore, the effects of O_2 flow rate are not obvious. When the operating current

density grows, the MHDCFC performance may be limited by the amount of oxygen supplied, and the O_2 flow rate becomes an influential factor.

3.6. Effect of cathodic pressure

Fig. 7 shows that the output voltage, efficiency and output power density, specific EOF and ECOP of MHDCFC increase with an increase in the cathodic pressure because both cathodic activation polarization loss and concentration polarization loss are decreased as the cathodic pressure increases. Conversely, the specific entropy production rate decreases as the cathodic pressure increases.

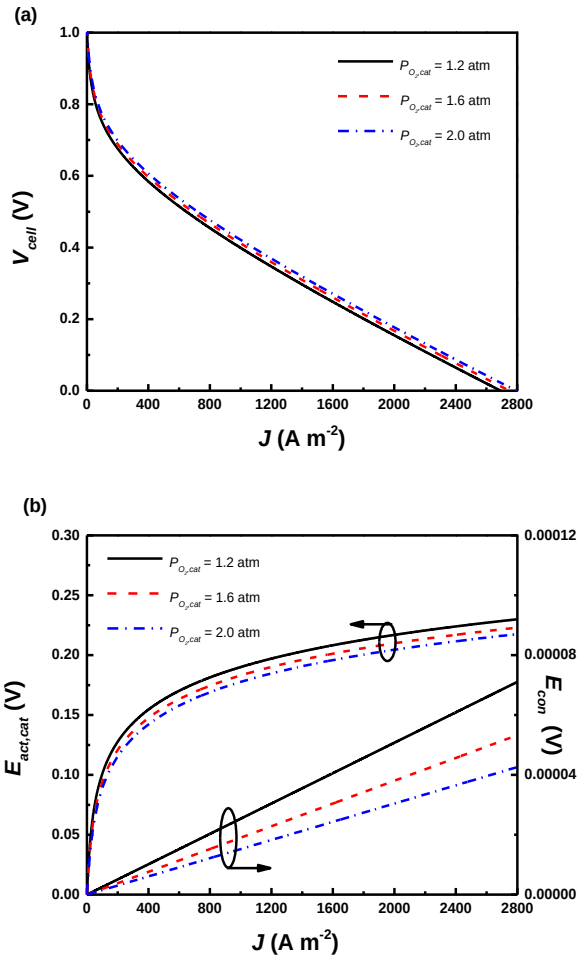

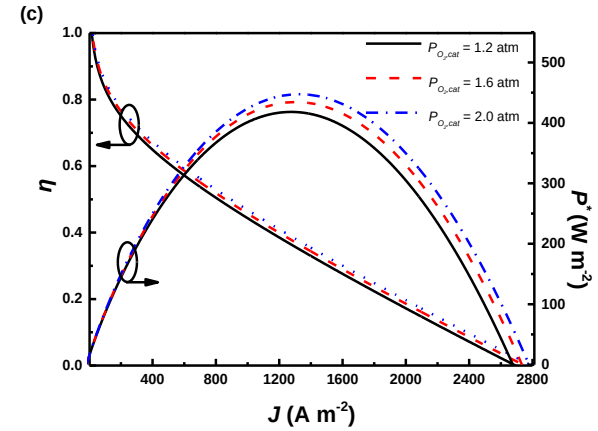
(c)
$P_{O_2,cat}$ = 1.2 atm
$P_{O_2,cat}$ = 1.6 atm
$P_{O_2,cat}$ = 2.0 atm
η
P^* (W m^{-2})
J (A m^{-2})

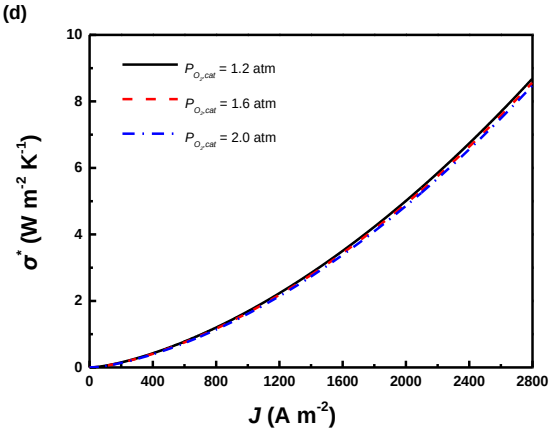
(d)
$P_{O_2,cat}$ = 1.2 atm
$P_{O_2,cat}$ = 1.6 atm
$P_{O_2,cat}$ = 2.0 atm
σ^* (W m^{-2} K^{-1})
J (A m^{-2})

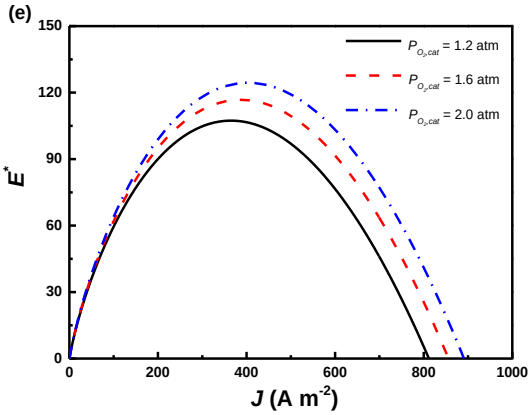
(e)
$P_{O_2,cat}$ = 1.2 atm
$P_{O_2,cat}$ = 1.6 atm
$P_{O_2,cat}$ = 2.0 atm
E^*
J (A m^{-2})

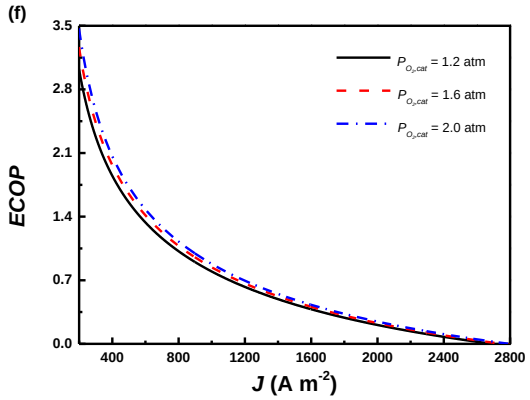

Figure 7. Effects of cathodic partial pressure on (a) output voltage, (b) cathodic activation polarization loss and concentration polarization loss, (c) efficiency and output power density, (d) specific entropy production rate, (e) specific EOF, and (f) ECOP.

This is because both cathodic activation polarization loss and concentration polarization loss are monotonically decreasing functions of cathodic oxygen concentration. Additionally, the OCV increases as the cathodic pressure increases. Practically, the partial pressure in the anodic chamber is greater than that in the cathodic chamber to prevent oxygen from diffusing into the anodic chamber.

3.7. Effect of reaction chamber width

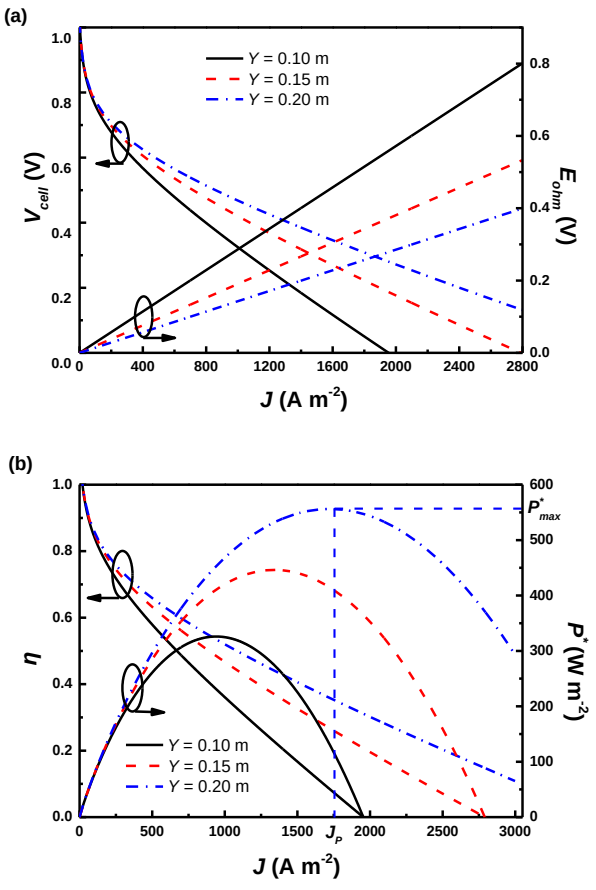

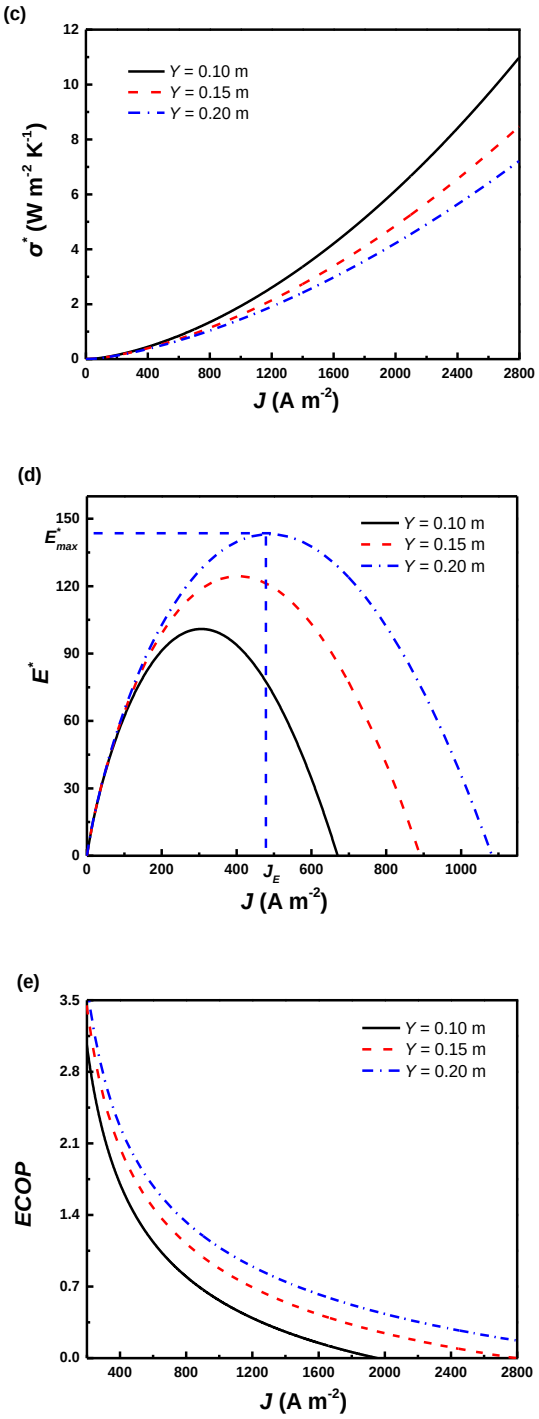

Figure 8. Effects of reaction chamber width on (a) output voltage and ohmic polarization loss, (b) efficiency and output power density, (c) specific entropy production rate, (d) specific EOF, and (e) ECOP.

As shown in Fig. 8, the output voltage, efficiency, output power density and specific EOF and ECOP of MHDCFC increase with the increase of the reaction chamber width, while the ohmic polarization loss and specific entropy production rate decrease as the reaction chamber width increases. This is because both anodic chamber resistance and cathodic chamber resistance of the MHDCFC are in

inversely proportional to the reaction chamber width. An increase in reaction chamber width results in a decrease in the ohmic polarization loss and an improvement in the MHDCFC performance. In addition, the effects of reaction chamber width are more significant with the increasing operating current density, and the range of operating current density of MHDCFC as well as J_P and J_E increase as the reaction chamber width increases.

4. CONCLUSION

To overcome the electrolyte carbonation problem, an MHDCFC model with asymmetric anode and cathode is put forward. Considering various thermodynamic and electrochemical losses, the MHDCFC model is mathematically described. Model validation shows that the present MHDCFC model is valid and reliable. The performance of MHDCFC is comprehensively evaluated by adopting output voltage, efficiency, power output, entropy production rate, EOF and ECOP as objective functions. The efficiency, power output, EOF and ECOP are in proportional to output voltage, while the entropy production rate is in inversely proportional to the output voltage. Exhaustive parametric studies show that the operating temperature, anodic and/or cathodic chamber heights, cathodic pressure, and reaction chamber width positively improve the MHDCFC performance, while fuel mass and O_2 flow rate have negative impacts on the MHDCFC performance. The obtained results are helpful for designing and operating such an actual MHDCFC.

ACKNOWLEDGMENTS
This work has been supported by the Natural Science Foundation of Zhejiang Province (Grant No. LY20E060002), and the K. C. Wong Magna Fund in Ningbo University, China.

References

1. J. Liu, *Prog. Chem.*, 18 (2006) 1027.
2. C. Li, Y.X. Shi and N.S. Cai, *J. Energ. Eng-asce.*, 1 (2007) 1.
3. S.P.S. Badwal and S. Giddey, *Mater. Forum.*, 34 (2010) 181.
4. S. Zecevic, E.M. Patton and P. Parhami, *Engineering and Technology*, 23 (2005).
5. S. Giddey, S.P.S. Badwal, A. Kulkarni and C. Munnings, *Prog. Energy Combust. Sci.*, 38 (2012) 360.
6. J.F. Cooper, Springer: New York (2007).
7. J. Zhang, X. Jiang, G. Piao, H. Yang and Z. Zhong, *Int. J. Hydrogen Energ.*, 40 (2015) 3321.
8. H. Zhang, G. Lin and J. Chen, *Int. J. Hydrogen Energ.*, 37 (2012) 3438.
9. N.J. Cherepy, R. Krueger, K.J. Fiet, A.F. Jankowski and J.F. Cooper, *J. Electrochem. Soc.*, 152 (2005) 80.
10. K. Hemmes, M. Houwing and N. Woudstra, *J. Fuel Cell Sci. Tech.*, 7 (2010) 051008.
11. A. Elleuch, A. Boussetta and K. Halouani, *J. Electroanal. Chem.*, 668 (2012) 99.
12. A. Kacprzak, R. Kobyłecki, R. Włodarczyk and Z. Bis, *J. Power Sources*, 321 (2016) 233.
13. A. Kacprzak, R. Kobylecki and Z. Bis, *J. Power Sources*, 239 (2013) 409.
14. L. Guo, J.M. Calo, E. DiCocco and E.J. Bain, *Energ. Fuel*, 27 (2013) 1712.
15. R. Liu, C. Zhao, J. Li, F. Zeng, S. Wang and T. Wen, *J. Power Sources*, 195 (2010) 480.

16. K. Hemmes, J.F. Cooper and J.R. Selman, *Int. J. Hydrogen Energ.*, 38 (2013) 8503.
17. Y. Xie, Y. Tang and J. Liu, *J. Solid. State. Electr.*, 17 (2013) 121.
18. S. Giddey, S.P.S. Badwal, A. Kulkarni and C. Munnings, *Prog. Energ. Combust.*, 38 (2012) 360.
19. W.W. Jacques. US Patent No. 555, 551 (1896).
20. J.F. Cooper, Conference: *Engineering and Technology* 375 (2004).
21. D.G. Vutetakis, D.R. Skidmore and H.J. Byker, *J. Electrochem. Soc.*, 134 (1987) 3027.
22. P.V. Pesavento, US Patent No. 6, 260, 697 (2001).
23. H.A. Liebhafsky, E.J. Cairns and John Wiley & Sons Inc, New York (1968).
24. T. Nunoura, K. Dowaki, C. Fushimi, S. Allen, E. Mészáros and M.J. Antal, *Ind. Eng. Chem. Res.*, 46 (2007) 734.
25. J. Goret and B. Tremillon, *Electrochimacta.*, 12 (1967) 1065.
26. S. Zecevic, E.M. Patton and P. Parhami, *Carbon.*, 42 (2004) 1983.
27. Y. Zhao, C. Ou and J. Chen, *Int. J. Hydrogen Energ.*, 33 (2008) 4161.
28. A. Kacprzak, R. Kobyłecki, R. Włodarczyk and Z. Bis, *J. Power Sources*, 255 (2014) 179.
29. A. Kacprzak, K. obyłeckiR, R. Włodarczyk and Z. Bis, *J. Power Sources*, 321 (2016) 233.
30. S. Zecevic, E.M. Patton and P. Parhami, *Chem. Eng. Commun.*, 192 (2005) 1655.
31. G.A. Hackett, J.W. Zondlo and R. Svensson, *J. Power Sources*, 168 (2007) 111.
32. C.C. Chen and J.R. Selman, *J. Power Sources*, 353 (2017) 312.
33. P. Grimshaw, J.M. Calo, L. Guo and S.B. Podhoretz, *Energ. Fuel*, 28 (2014) 2272.
34. L. Guo, J.M. Calo, C. Kearney and P. Grimshaw, *Appl. Energ.*, 129 (2014) 32.
35. B.R. Alexander, R.E. Mitchell and T.M. Gür, *J. Power Sources*, 228 (2013) 132.
36. X. Li, Z. Zhu, R. De Marco, J. Bradley and A. Dicks, *J, Power Sources*, 195 (2010) 4051.
37. A. Kulkarni, F.T. Ciacchi, S. Giddey, C. Munnings, S.P.S. Badwal, J.A. Kimpton and D. Fini, *Int. J. Hydrogen Energ.*, 19 (2012) 92.
38. J.F. Cooper and K. Berner, The Carbon Fuel Cell Seminar, Palm Springs, CA, US: November 14 (2005).
39. L. Xing, J. Hao, X. Li, Y. Zhang, Z. Hu and Y. Gao, *J, Power Sources*, 363 (2017) 428.
40. Z. Wu, L. Chen, Y. Ge and F. Sun, *Front. Energy*, 13 (2019) 579.
41. L. Chen, F. Meng and F. Sun, *Cryogenics.*, 52 (2012) 58.
42. L. Chen, Y. Ge, X. Qin and Z. Xie, *Int. J. Heat Mass. Tran.*, 129 (2019) 855.
43. A. Bejan, *J. Appl. Phys.*, 79 (1996) 1191.
44. F.L. Curzou and B. Ahlborn, *Am. J. Phys.*, 43 (1975) 22.
45. F. Angulo-Brown, *J. Appl. Phys.*, 69 (1991) 7465.
46. L. Chen, F. Sun and W. Chen, *J. Eng. Therm. Energy and Pow.*, 9 (1994) 374.
47. L. Chen, J. Zhou and F. Sun, *Appl. Energ.*, 77 (2004) 327.
48. Y. Ust, B. Sahin and O.S. Sogut, *Appl. Energ.*, 82 (2005) 23.
49. H. Zhang, H. Xu, B. Chen, F. Dong and M. Ni, *Energy*, 132 (2017) 280.
50. A.A. Omelchuk, O.G. Zarubitskii, V.P. Opanasyuk, N.F. Zakharchenko, V. Ye and D. Yakov, *J. Appl. Electrochem.*, 33 (2003) 519.
51. K. Hemmes, M. Houwing and N. Woudstra, *J. Fuel Cell Sci. Tech.*, 7 (2010) 051008.
52. S.J. Liang and L.K. Ang, *Phys. Rev. Appl.*, 3 (2015) 014002.
53. Y. Zhao and J. Chen, *J. Power Sources*, 186 (2009) 96.
54. S.H. Chan, K.A. Khor and Z.T. Xia, *J. Power Sources*, 93 (2001) 130.
55. Q.H. Liu, Y. Tian, C. Xia, L.T. Thompson, B. Liang and Y.D. Li, *J. Power Sources*, 185 (2008) 1022.
56. J. Brouwer, F. Jabbari, E.M. Leal and T. Orr, *J. Power Sources*, 158 (2006) 213.
57. M. Baranak and H. Atakül, *J. Power Sources*, 172 (2007) 831.
58. L. Xing, J. Hao, Y. Zhang, Y. Gao, L. Li and Z. Cao, *Int. J. Energy Res.*, 1 (2019) 1.
59. A. Liu and Y. Weng, *J. Power Sources*, 195 (2010) 1872.
60. Z. Wu, P. Zhu, J. Yao, P. Tan, H. Xu, B. Chen, F. Yang, Z. Zhang and M. Ni, *Energy*, 192 (2019)

116613.
61. F. Ishak, I. Dincer and C. Zamfirescu, *J. Power Sources*, 212 (2012) 73.
62. B. Basio, E. Arato and P. Costa, *J. Power Sources*, 115 (2003) 189.
63. M. Paidar, K. Bouzek and H. Bergmann, *Chem. Eng. J.*, 85 (2002) 99.

© 2020 The Authors. Published by ESG (www.electrochemsci.org). This article is an open access article distributed under the terms and conditions of the Creative Commons Attribution license (http://creativecommons.org/licenses/by/4.0/).